Arabian Journal of Chemistry (2023) 16, 104405

King Saud University

Arabian Journal of Chemistry

www.ksu.edu.sa
www.sciencedirect.com

ORIGINAL ARTICLE

Increasing the accuracy of estimating the dynamic viscosity of hybrid nano-lubricants containing MWCNT-MgO by optimizing using an artificial neural network

Mohammad Hemmat Esfe [a,*], Saeed Esfandeh [a], Fatemeh Amoozadkhalili [a], Davood Toghraie [b,*]

[a] *Nanofluid Advanced Research Team, Tehran, Iran*
[b] *Department of Mechanical Engineering, Khomeinishahr Branch, Islamic Azad University, Khomeinishahr, Iran*

Received 27 June 2022; accepted 6 November 2022
Available online 12 November 2022

KEYWORDS

ANN;
Experimental data;
Hybrid nano-lubricants;
Dynamic viscosity;
nanolubricant;
Levenberg-Marquardt;
multilayer perceptron

Abstract Artificial neural network (ANN) is utilized as efficient models to forecast the nanofluids (NFs) viscosity (μ_{nf}). In this examination, ANN is used to forecast the μ_{nf} of the MWCNT-MgO (25 % –75 %) / SAE40 nano-lubricant (NL) experimental data set. Experimental evaluation of NLs is taken in volume fraction of nanoparticles (NPs) $\varphi = 0.0625$ % –1% and temperature range of T = 25 to 50 °C. To predict the μ_{nf} of the data using ANN, a multilayer perceptron (MLP) ANN with the algorithm of Levenberg-Marquardt (LM) is utilized. For ANN modeling, temperature, φ and shear rate ($\dot{\gamma}$) are determined as inputs and μ_{nf} is determined as output. From 400 various ANN samples for NL, the optimal sample (OS) is selected, comprising two hidden layers (HLs) with the OS of 8 and 5 neurons in the primary and second layer, respectively. Eventually, for the OS, the amount of the regression coefficient (RC) and the mean square error (MSE) are set equal to 0.9999882 and 0.001453292, respectively. The margin of deviation (MOD) for all ANN information is in the range of less than –1% < MOD < +1%. It's good because the ANN pattern is more precise and has a great ability to forecast μ_{nf}. The main goal of this research is to model and estimate

* Corresponding authors.
E-mail addresses: m.hemmatesfeh@gmail.com (M. Hemmat Esfe), Toghraee@iaukhsh.ac.ir (D. Toghraie).
Peer review under responsibility of King Saud University.

ELSEVIER Production and hosting by Elsevier

https://doi.org/10.1016/j.arabjc.2022.104405

the μ_{nf} of MWCNT-MgO (25:75)/SAE40 NL through ANN and also to select the optimal structure from the set of predicted ANN structures and manage time and cost.

1. Introduction

The flourishing time of nanoscience can be seen in the last two decades, where the research of researchers regarding nanoscience has found a significant improvement in all fields of science. Researchers are continuously investigating various aspects of this branch of technology (Doaa Domyati et al., 2022), (Azin et al., 2021), (Zhang.et al., 2015), (Wang et al., 2022), (Anqi et al., 2022). Investigating the rheological properties of fluids has always been one of the subjects of researchers' research, and the reduction of viscosity to reduce pumping power has always become one of the subjects of researchers' research Zhang et al., (2022a), Zhang et al., (2022b). Also, fluids are used in various applications such as lubrication, heat transfer, etc. and optimizing their properties, such as increasing the thermal conductivity and reducing the viscosity, can increase their efficiency Bagheri et al., 2020; Esfe, 2017; Keshtegar et al., 2020; Li et al., 2022; Putra, 2020; Rikani, 2021; Tang et al., 2022; Yang et al., 2017. The particles that are added to fluids in old research had micrometer sizes. These particles do not have the necessary stability in the suspension and the settling speed of these materials is high, and this causes the fluid passages to be blocked quickly. But over time, nanofluids (NFs) were obtained by distributing particles with nano dimensions in conventional fluids. NFs are new materials that are a combination of nanoparticles (NPs) with a size of 0–100 nm in the base fluid Hosseini and Dehaj, 2021a,b; Mousavi et al., 2021; Sheikholeslami, 2017; Valipour et al., 2017 while that NFs form a much more stable suspension and their low sedimentation speed minimizes the problem of clogging and blockage of ducts. These particles are made of metal particles such as copper (Cu), magnesium (Mg) or metal oxides such as Al_2O_3 and CuO and Khanafer et al., (2012), Saidur et al., (2011), Haddad et al., (2012). NFs originate from heat transfer (HT) and nanotechnology. NFs have superior properties, and this has led to an increase in cooling power, a reduction in the power required for fluid pumping, the development of more compact NF-based systems, a reduction in the ratio of cooling fluids, a reduction in friction coefficient, and miniaturization of heat exchangers. size and improved wear resistance (see Fig. 1).

One of the main advantages of NFs can be sought in heat exchangers. Since thermal conductivity (TC) augmentation is much more significant in NFs Azman et al., (2021), Öğüt and Kahveci, (2016), Jamei et al., 2021; Ruhani, 2022; Yang et al., 2021, the HT coefficient of NFs passing through the heat exchanger tubes is expected to enhance significantly Nfawa et al., (2021). Studies have proven that the addition of NPs to fluids, can enhance the μ_{nf} Banisharif et al., 2021; Dezfulizadeh et al., 2021; Esfe and Sarlak, 2017; He, 2020; Hosseini and Dehaj, 2021a,b; Shahsavar et al., 2021. If two or more NPs are added to the fluid, then hybrid NFs will be created that can have better properties than NFs with a single NP. This NF is generally prepared by dispersing two different NPs in the base fluid and appears as new nanotechnology. One of the pioneers in the field of hybrid NFs that has worked on many NFs is the Hemmat Esfe research team, which has examined thermophysical features like μ_{nf} and TC Hemmat Esfe et al., 2022, Esfe and Arani, 2018; Fontes et al., 2015; Kotia and Ghosh, 2015. Hybrid NFs are used in various fields such as heat exchangers and electric coolers, the automotive industry, medicine and defense Jamil et al., (2020), Alidoust et al., (2022). Table 1 lists the studies on μ_{nf} and TC of NFs.

For utilization of the properties of NFs in the needed calculations in industrial system designs, it is necessary to present these properties in form of mathematical equations or software. Some studies have provided some theoretical and experimental equations, based on temperature and φ. These studies are listed in Tables 2 and 3. Also, researchers used software methods for the prediction of these properties. Their results indicate the high precision of these methods and their flexibility to changing conditions Goudarzi et al., (2009), Goudarzi et al., (2008), Ashrafi et al., (2018).

The rheological behavior of fluids is a science that deals with the deformation of materials due to the exerted forces on them. Determination of φ and temperature that affects on properties of NFs is one of the aspects of rheology science that was the subject of some studies in recent years. NFs have two Newtonian and non-Newtonian behaviors depending on the type of used materials in them. Aberoumand et al. Aberoumand et al., (2016) measured the μ_{nf} of Ag/oil NL at T = 25 to 60 ℃ and $\varphi = 0.12$ % to 0.72 %. The outcomes display that with an increase in φ, the μ_{nf} changes shift from linear to non-linear modes; in other words, the NL's behavior becomes non-Newtonian. Also, at T < 35 ℃, NFs show

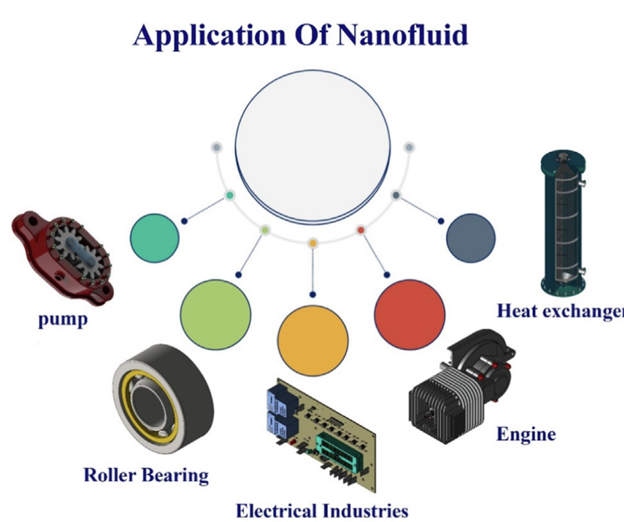

Fig. 1 Applications of NFs.

Table 1 Some of the recently examinations on the NFs.

Ref.	NPs	Base Fluid	T (C)	φ(%)	The purpose of the Experiment
Akhavan-Behabadi et al., (2016)	Al_2O_3	Gear oil (SAE EP-90)	15–40	0–2	Distribution of size and stability with varying temperatures and φ
Binu et al., (2015)	Diamond & MWCNT	Oil	20 & 25	0.005–0.05	k_{nf}, μ_{nf} and breakdown voltage of NFs with varying φ
Aberoumand et al., (2016)	CuO	Oil	20–80	0.5–1.5	Thermophysical features and convective HT rate
Barati-Harooni et al., (2016)	TiO_2	Oil	10–80	0.05–2.5	Correlation and μ_{nf}
Çolak et al., (2021)	Ag	oil	40–100	0–0.72	μ_{nf} with varying φ.

Table 2 Some of the theoretical models.

Ref.	$\varphi\Phi$(%)	Correlation
Einstein(1905)	———	$\frac{\mu_{nf}}{\mu_{bf}} = \boldsymbol{e}^{\left(\frac{2.5\varphi}{1-\boldsymbol{k}\varphi}\right)}$ $1.35 < k < 1.91$
Krieger and Dougherty (1959)	———	$\frac{\mu_{nf}}{\mu_{bf}} = \frac{1}{(1-\varphi)^{2.5}}$
Nielsen(1970)	< 2	$\frac{\mu_{nf}}{\mu_{bf}} = (1 + 2.5\,\varphi)$
Lundgren(1972)	———	$\frac{\mu_{nf}}{\mu_{bf}} = [1 - \varphi_m] - 2.5$ $\varphi_m 0.495 < \varphi_m < 0.54$
Wanget al., (1999)	< 2	$\frac{\mu_{nf}}{\mu_{bf}} = (1 + 1.5\varphi)e^{\left(\frac{1}{1-\varphi_m}\right)}$
Tsenget al., (2003)	< 4	$\frac{\mu_{nf}}{\mu_{bf}} = (1 + 2.5\ \varphi + 6.25\ \varphi^2)$
Meybodiet al., (2016)	———	$\frac{\mu_{nf}}{\mu_{bf}} = (1 + 7.3\varphi + 123\varphi^2)$

non-Newtonian behavior but at T > 35 ℃, it begins to show Newtonian behaviors. A review of past research shows that the need for high accuracy in the process of estimating the μ_{nf}, especially hybrid NFs, is of great importance. Therefore, recently the use of ANNs and other post-processing methods were widely studied by researchers. In recent years, ANN was used in various applications such as solar cells, memristors, thermistors, and supercapacitors, in medicine, including data prediction in the covid-19 virus, etc that can be find in Shakeri et al., (2016), Sutar et al., (2021), Dongale et al., (2015), Yan et al., (2020), Zhang et al., (2021), , Safa et al., (2020) studies and some of them are shown in Fig. 2.

In recent years, increasing the accuracy in predicting the rheological behavior of NFs and nano-particles was one of the most important fields of study in the field of HT. Considering that the behavior of NFs and NLs should be studied separately, it is necessary to define a wide range of targeted studies to increase the accuracy of predicting the rheological and thermal behavior by different researchers and its results in industrial and engineering simulations. For this reason, using experimental data, μ_{nf} of MWCNT-MgO(25:75)/SAE40 is presented in terms of temperature, φ and $\dot{\gamma}$ variables by ANN. It should be noted that all experimental data were taken from (Hemmat Esfe et al., 2022). The complex rheological behavior of this NL and the presence of different parameters reduce the accuracy of common relationships for predicting μ_{nf}. The optimal ANN is selected after examining a large number of neurons and different transfer functions in a large number of different ANNs. According to the authors, no published research has been presented in this area so far.

2. ANN training

An ANN is fabricated of a set of nodes named artificial neurons that are like biological neurons in the brain of a human. Any connection among neurons can transfer a signal from one neuron to another Esfe et al., 2018; Rezaee et al., 2018. Signals and then the signal neurons are connected to their process by the receiving neuron. In the ordinary implementation of ANNs, a signal of the synapse is an actual number, and each neuron output is computed using a nonlinear function of its input. Synapses and neurons have weights that are regulated

Table 3 Some of the experimental models.

Ref.	NF	φ (%)	Correlation
Esfe et al. (2014)	Al_2O_3, TiO_2, SiO_2 and CuO/Water	< 4	$\frac{\mu_{nf}}{\mu_{bf}} = \frac{133.546-343.824e^{\left(\frac{\varphi}{s}\right)}+290.118\left(e^{\left(\frac{\varphi}{s}\right)}\right)^2-78.993\left(e^{\left(\frac{\varphi}{s}\right)}\right)^3}{0.911+32.3301\times\frac{\ln s}{T}-11.732\times\frac{(\ln s)^2}{T}}$
Esfe and Saedodin (2014)	ZnO/EG	Up to 2	$\frac{\mu_{nf}}{\mu_{bf}} = (0.9118e^{5.49\varphi-0.00001359T^2} + 0.0303\ln(T))$
Afrand et al., (2016)	$Mg(OH)_2$/ EG	< 2	$\frac{\mu_{nf}}{\mu_{bf}} = (15.89 + 614.4\varphi - 14526\varphi^2)$
Shaddel et al., (2016)	Ag/Oil	0–0.72 (wt)	$\frac{\mu_{nf}}{\mu_{bf}} = (1.15 + 1.061\varphi - 0.5442\varphi^2 + 0.1181\varphi^3)$
(Hemmat Esfe et al., 2022)	MWCNT-MgO	up to 1	$\mu_{nf} = +1439.18463–74.55874T + 680.60734\varphi-0.023008SR-18.93092T*\varphi + 9.20862E-004T*SR + 1.41458T^2-335.84851SVF^2 + 1.64364E-007SR^2 + 0.14964T^2\varphi-1.03952E-005\ T^2*SR + 3.83013\ T*\varphi^2-9.38513E-003\ T^3 + 68.56743\varphi^3$

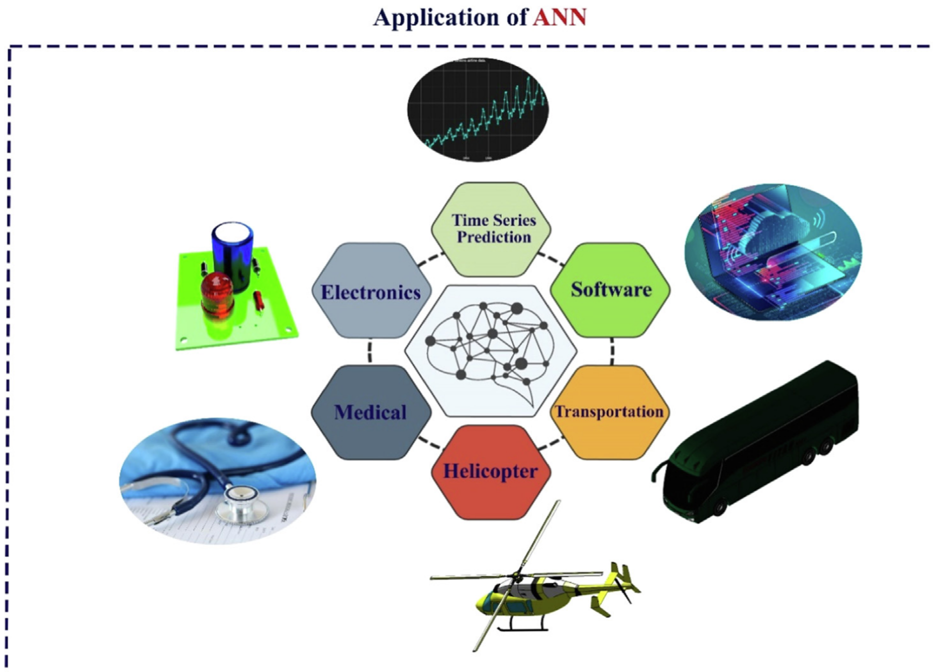

Fig. 2 Various applications of anns in various industries.

as learning progress Shirani et al., (2015), Aghaei et al., (2018), Ghazvini et al., (2020), Dianati Tilaki et al., (2020), Rustamovich Sultanbekov et al., (2020), Tan et al., (2022), Ruhani et al., (2019a), Ruhani et al., (2019b). In this research, ANN modeling to predict the μ_{nf} of MWCNT-MgO (25 %-75 %)/SAE40 in φ, temperature and $\dot{\gamma}$ are determined as inputs and μ_{nf} is determined as output. An example of an ANN structure is a structure with two hidden layers (HLs), in which there are 10 neurons in each HL and using transfer functions (TFs) (4 modes) which are composed of a total of 400 topologies. The ANN pattern is a multilayer perceptron (MLP) and the utilized algorithm for the training section is Levenberg-Marquardt (LM). The sigmoid transfer function is utilized in each of the HLs. To choose, the most optimal sample (OS) of ANN, a set of 400 various ANN samples was investigated, which vary in the neurons number in the primary and second HLs and the mixture of exerted TFs to the HLs. In the examined samples, various mixtures of tan-*sigmoid* and log-*sigmoid tangent* TFs in HLs were utilized. Out of 400 different ANN structures, the OS is formed, which includes two HLs with

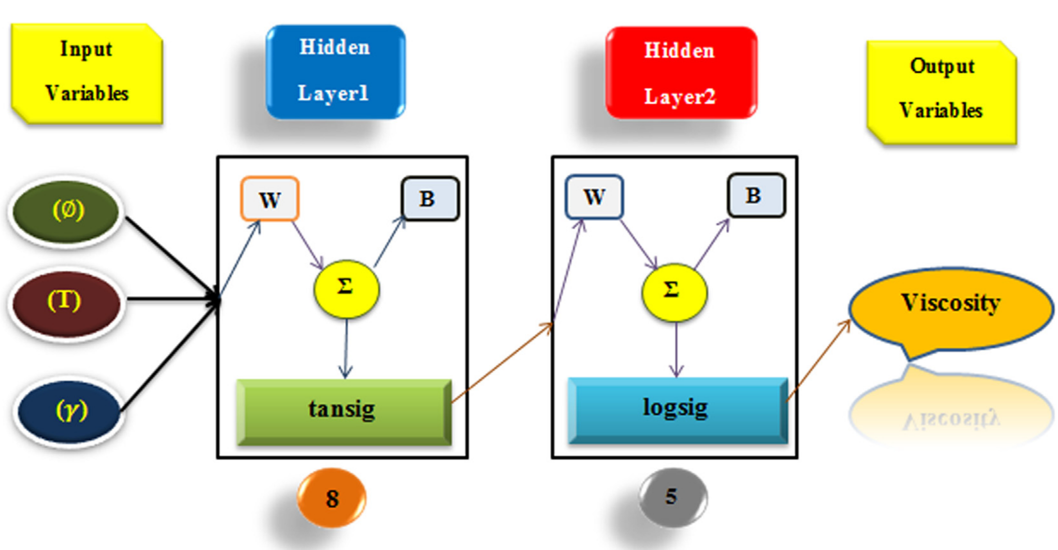

Fig. 3 The best ANN.

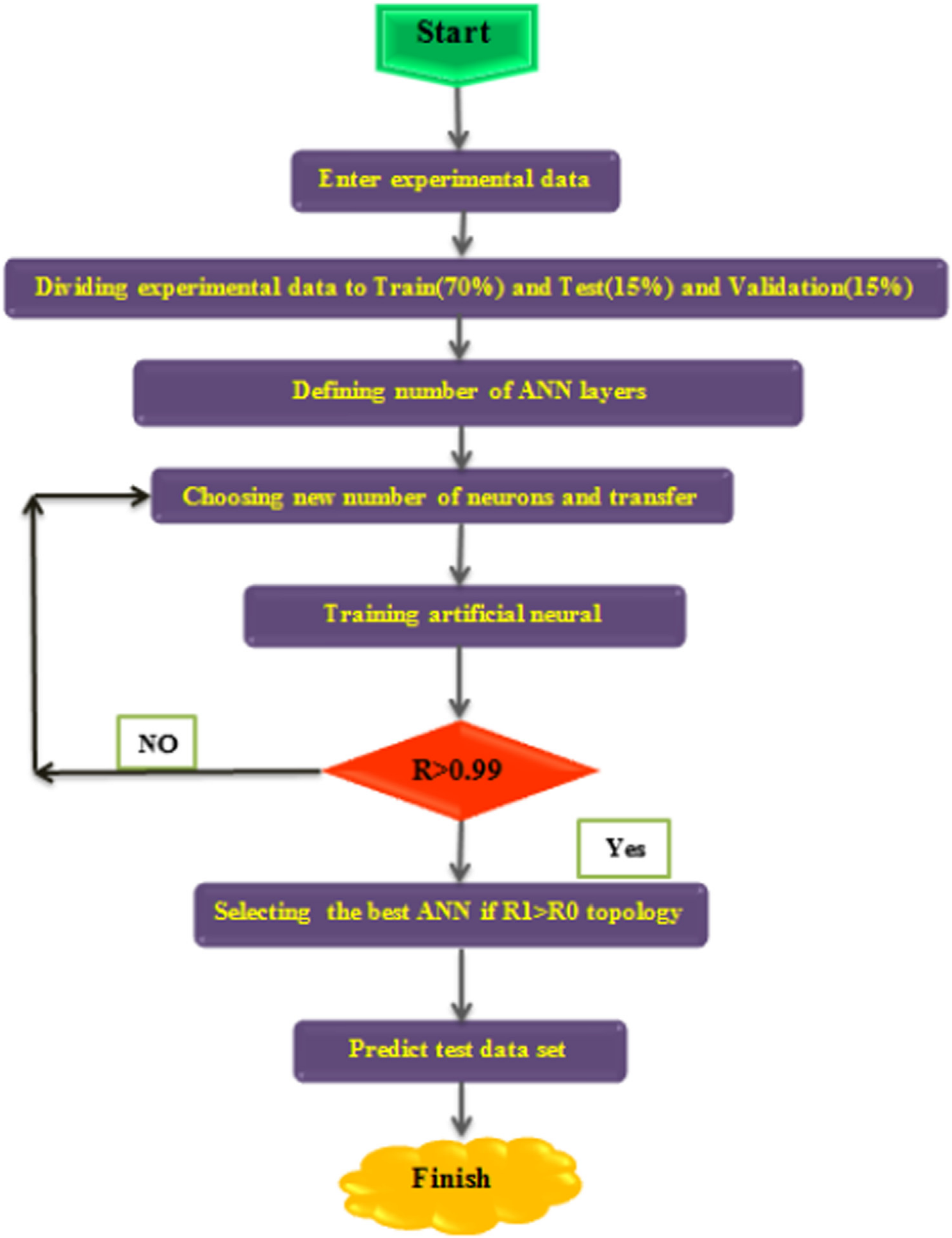

Fig. 4 The proposed algorithm to attain the OS of ANN.

Table 4 Features of top 11 ANN structures.

Candidate Topology No.	Structure	Function1	Function2	R	Train R	Val R	Test R
1	[2 2]	tansig	tansig	0.9999282	0.9999531	0.9999695	0.9998892
2	[2 4]	tansig	tansig	0.9999611	0.9999725	0.9999321	0.999487
3	[2 5]	tansig	tansig	0.9999651	0.9999742	0.9999254	0.9999670
4	[2 6]	logsig	tansig	0.9999668	0.9999766	0.9999556	0.9999264
5	[2 8]	tansig	logsig	0.9999753	0.9999800	0.9999703	0.9999626
6	[3 4]	logsig	tansig	0.9999754	0.9999781	0.9999683	0.9999624
7	[4 2]	tansig	tansig	0.9999757	0.9999762	0.9999766	0.9999702
8	[4 5]	logsig	tansig	0.9999836	0.9999883	0.9999734	0.9999766
9	[4 6]	tansig	logsig	0.9999843	0.9999888	0.9999839	0.9999642
10	[7 4]	tansig	tansig	0.9999851	0.9999956	0.9999704	0.9999519
11	[8 5]	tansig	logsig	0.9999882	0.9999962	0.9999712	0.9999709

the OS of 8 and 5 neurons in the primary and second layers, respectively. In each section, the number of HLs, the neuron number in each HL, and the related TFs to the HLs were put on the agenda to determine the structure of the set of ANN structures. The technique of weighting exerted on neurons is also assessed randomly. Finally, to attain the OS and by the training process of ANN, 174 sets of information were utilized, which were allocated to three stages, information to train (70 %), validation step to optimize the neurons number, and HLs (15 %) and test step to the modality of performance of ANN (15 %). The best-choose sample from the 400 examined samples to forecast the μ_{nf} of MWCNT-MgO (25:75) / SAE40 NL is plotted in Fig. 3. Fig. 4 shows the flowchart for choosing and gaging the 400 structures' performance of the examined ANN. Gaging the amount of R and reaching the number 1 is one of the chief measures for choosing the finest ANN sample. A higher R-amount is a symbol that ANN outcomes are more consonant with laboratory outcomes.

Given that the ANN alone cannot use all the modeled structures, it is necessary to assess ANN's performance. Therefore, the ANN regression coefficient (RC) factors R for the three steps are presented in Table 4 and the best amount of

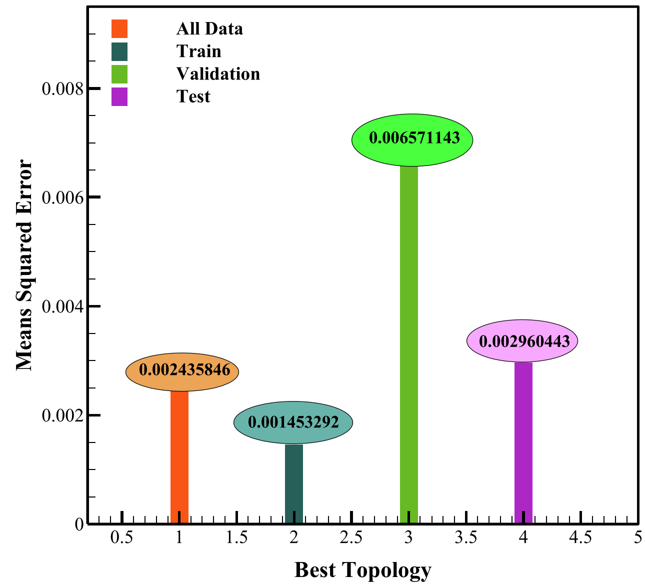

Fig. 6 The MSE applying HL neurons.

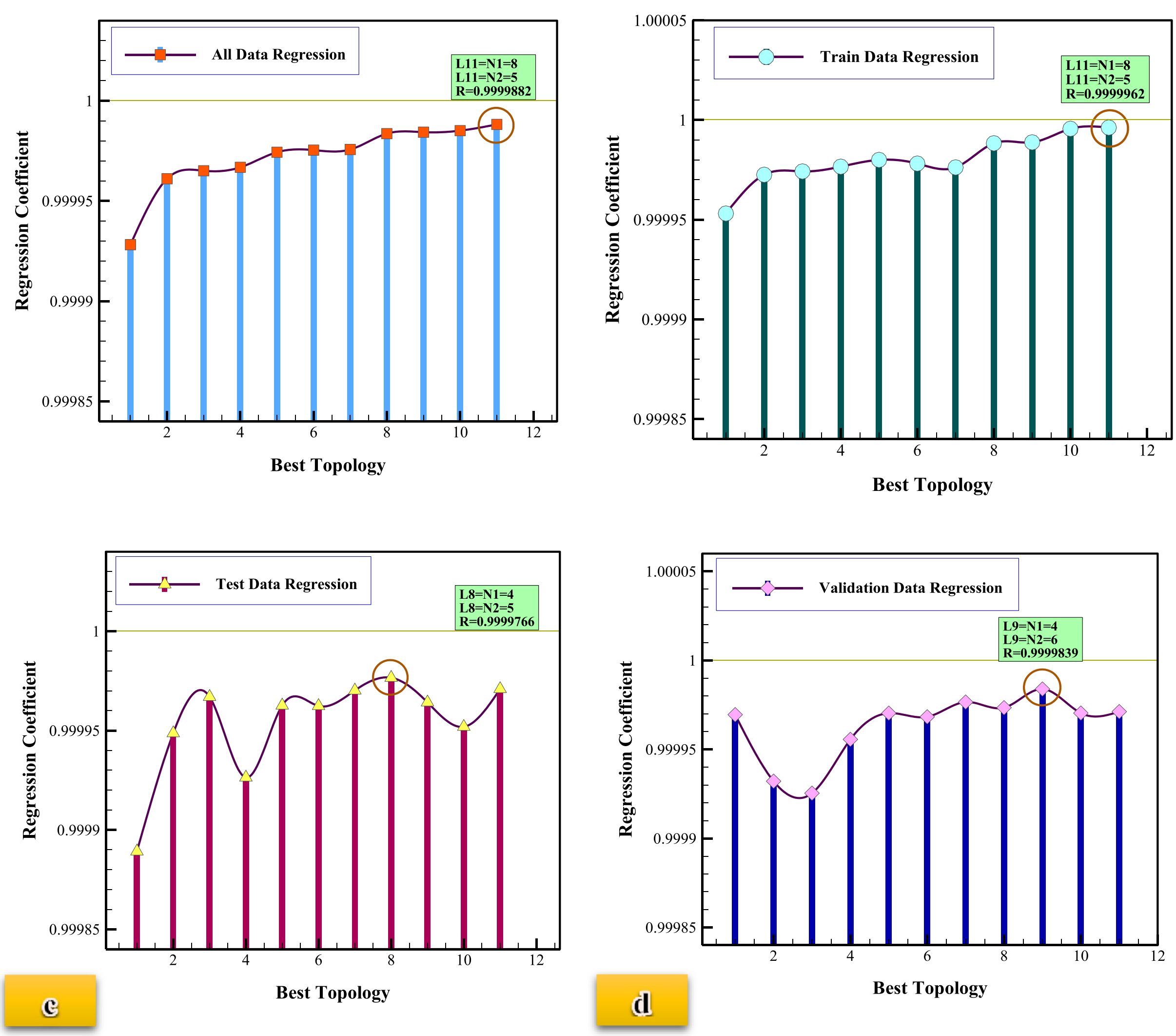

Fig. 5 The RC applying HL neurons.

the RC based on the information in Table 4 is equal to 0.9999882, which is related to the eleventh structure in Table 4. It must be mentioned that the eleventh structure in Table 1 is the OS among the 400 samples with maximum RCs compared to other examined samples. The neuron's number and the kind of TFs are given in Table 4.

3. Results and discussion

After determining the OS and neuron number and HLs from the set of different samples of the ANN, in this section, it is essential to examine the performance of the forecasted information from different aspects. The amount of the RC close to 1 indicates a close connection between the laboratory and the forecasted information from the ANN. The correlation relationship for different stages including training, testing, and validation and all information is drawn in Fig. 5 in four separate sections. Note that the RC for all information in the current pattern is higher than 0.999. Although the RC occurred in the ninth or eighth topologies during the training and validation steps, here, the results of the RC survey are more important for all data, which is 0.9999882 and belongs to the 11th proposed topology.

The performance of the selected sample from ANN samples in terms of Mean-Square Error (MSE) in three stages (Train, test, and validation) and all information analysis is displayed in Fig. 6. The MSE in the training phase compared to the other phases is the lowest MSE, which according to Eq. (1) is equal to 0.001453292.

$$MSE = \frac{1}{N}\sum_{i=1}^{N}\left(\mu_{rel}|_{EXP} - \mu_{rel}|_{pred}\right)^2 \quad (1)$$

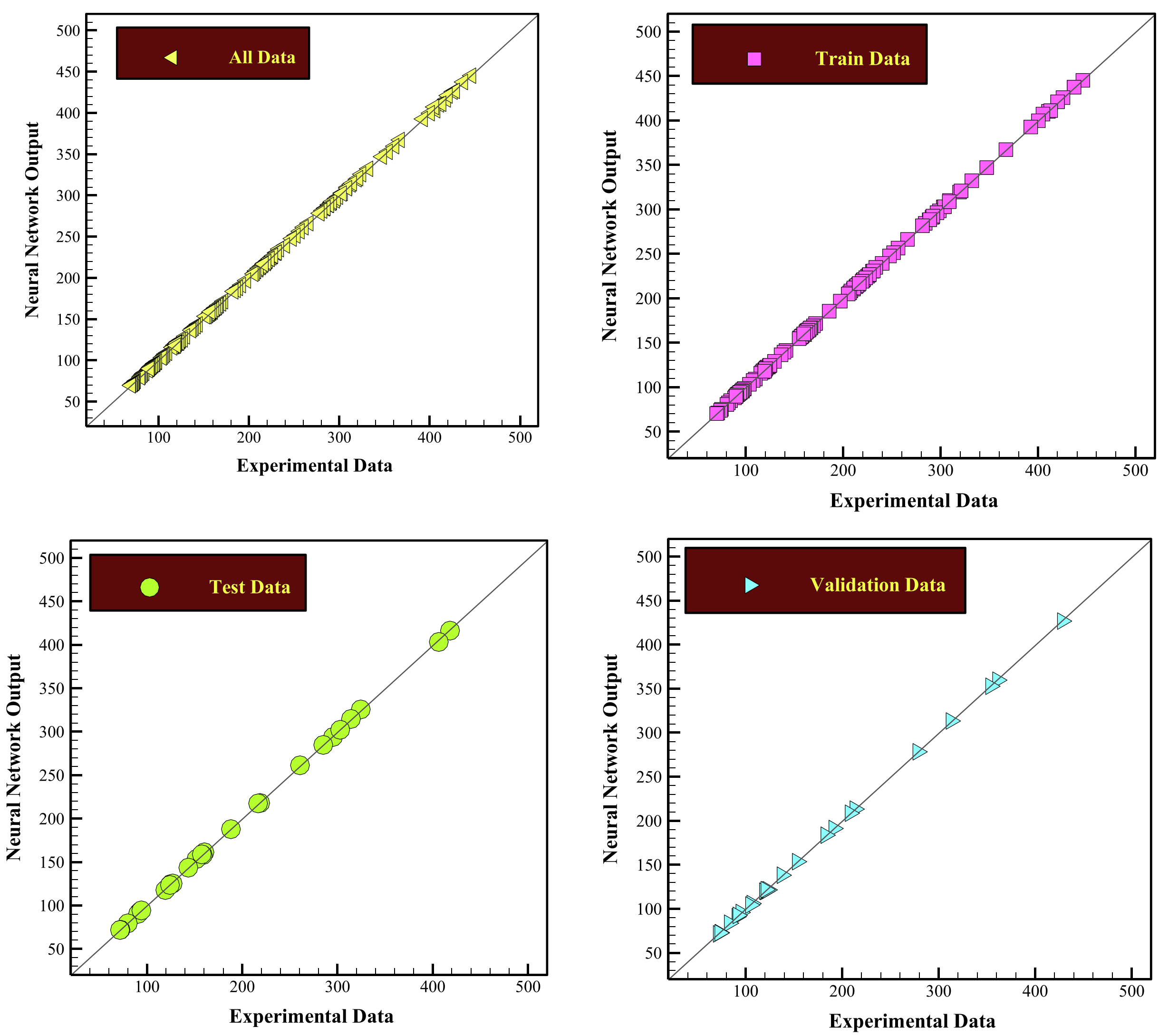

Fig. 7 Comparison among forecasted information with ANN-according to empirical information.

The evaluation of the forecasted information of the designated ANNs with the outcomes of the experimental information in four sectors (All information, training, validation, and test) is drawn in Fig. 7. According to Fig. 7, there is a very good homogeneity among the outputs of ANN data and experimental data, and the modeled data accurately predicts the laboratory values.

A comparison between experimental data predicted by ANN is shown in Fig. 8. This was done numerically in three stages including training, testing, and validation. If adequate accuracy is achieved in the data, the ANN training is complete and provides an acceptable output. According to the curves in Fig. 8, There is a close correlation between the data, which indicates the high accuracy of the ANN data from the experimental data.

Fig. 9 shows another comparison between the experimental and the forecasted information using the ANN in different temperature ranges and for each φ separately. As shown in the curves of Fig. 9, all points predicted using ANN are associated with points of experimental, which indicate the high precision and appropriate ANNs performance in forecasting laboratory information.

Fig. 10 shows the associated error with the predicted data of different phases of the train, validation, and testing for the data set separately. As shown in Fig. 10, the maximum error is between $\pm$ 2 and this indicates the accuracy of predicted viscosities from the ANN model. According to Fig. 10, it was observed that the highest error in all data and test phases is seen at T = 250 ^{0}C and less than 5$\pm$. The least error in the validation phase is less than $\pm$ 1.

A histogram diagram of data prediction errors of the three phases in ANN modeling is shown in Fig. 11. Most of the data errors are positioned near the line passing through zero and in the range of $\pm$ 1. However, for the test and validation phases, the frequency of data was considered in the range of more than $\pm$ 1.5. According to Fig. 11, the least error with the highest frequency belongs to the training phase which is equal to −0.152232464. Also to check the accuracy of the ANN prediction, the margin of deviation (MOD) is calculated and depicted in Fig. 12.

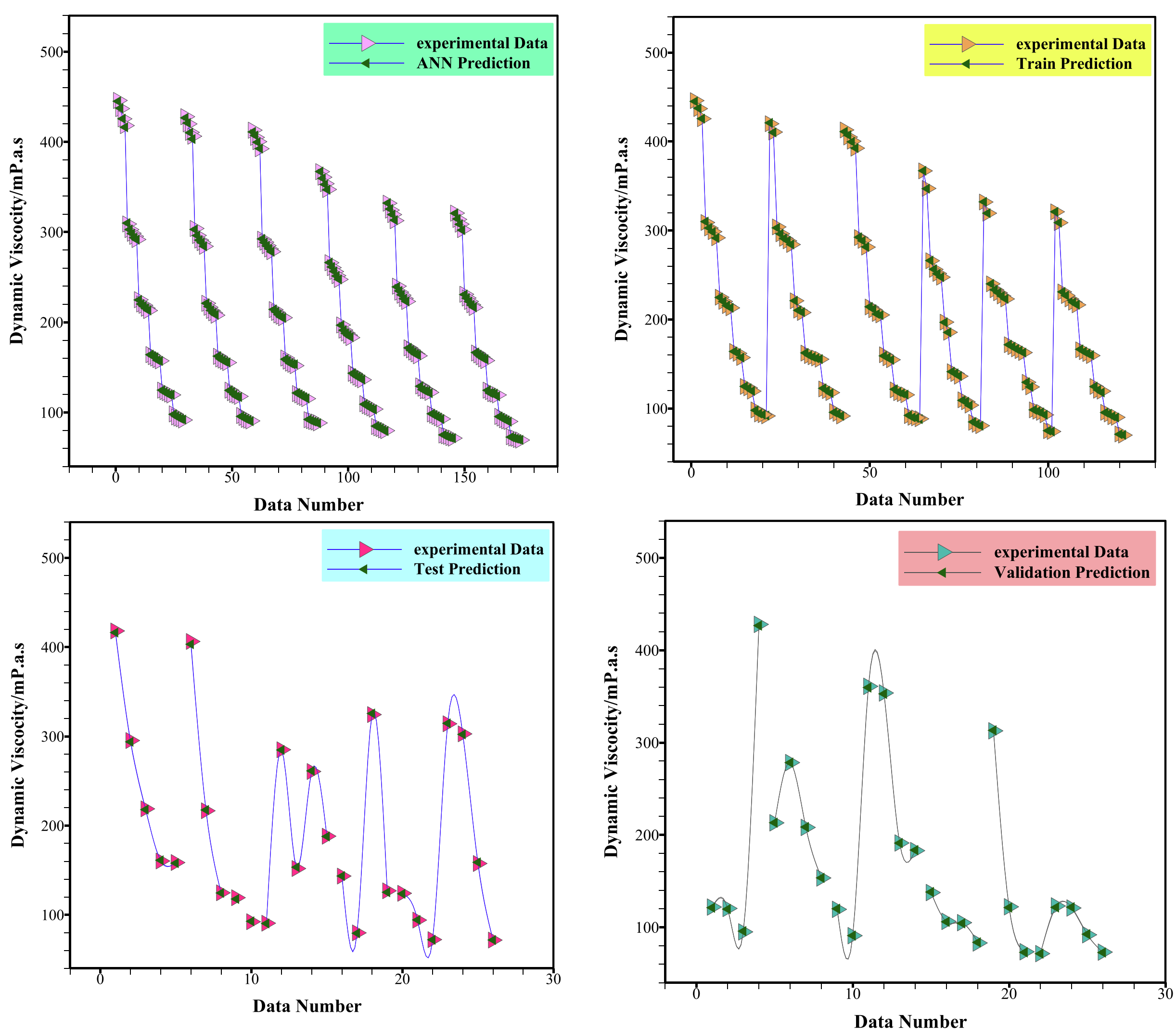

Fig. 8 ANN accuracy.

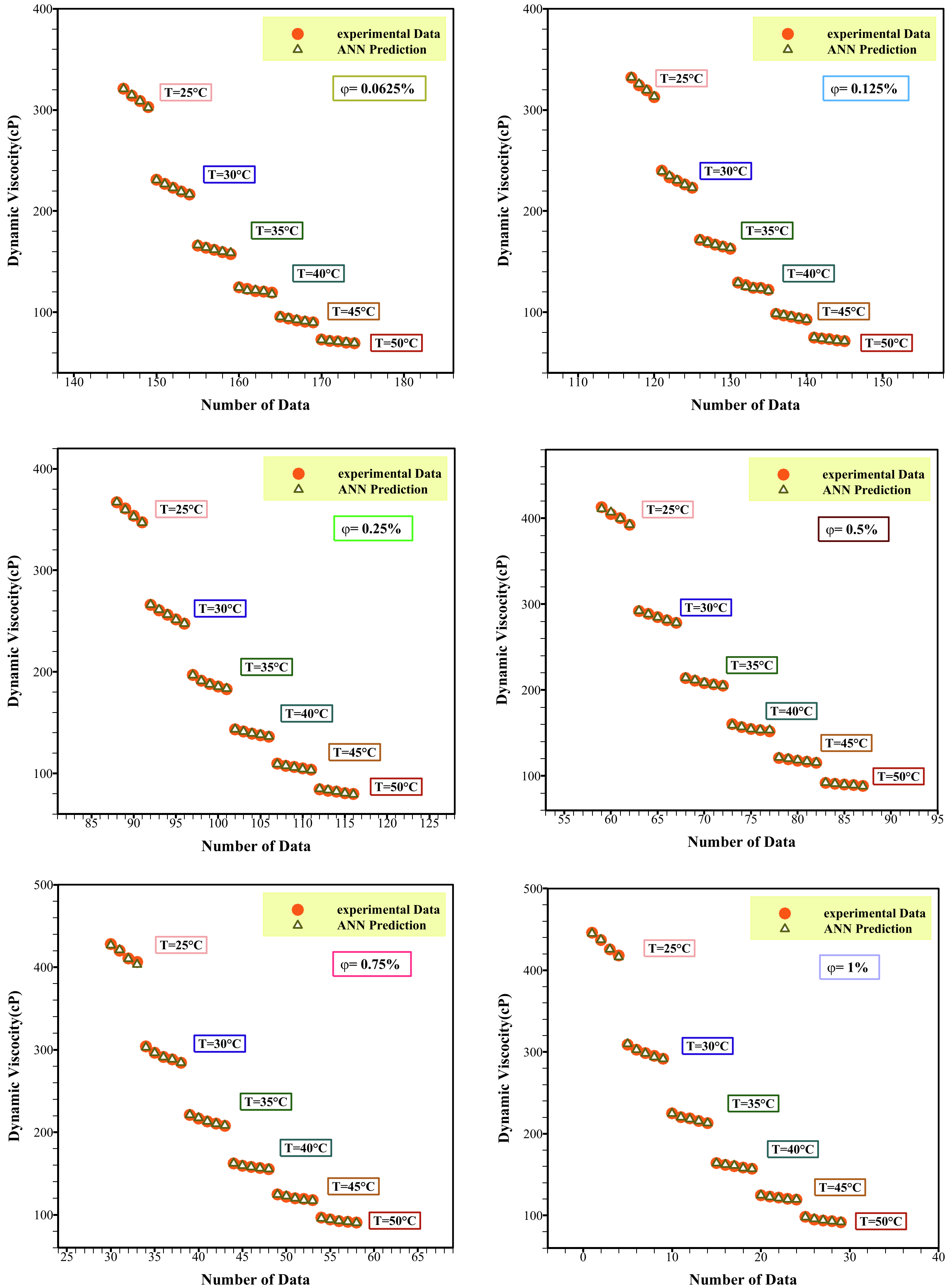

Fig. 9 Comparison of ANN by experimental information.

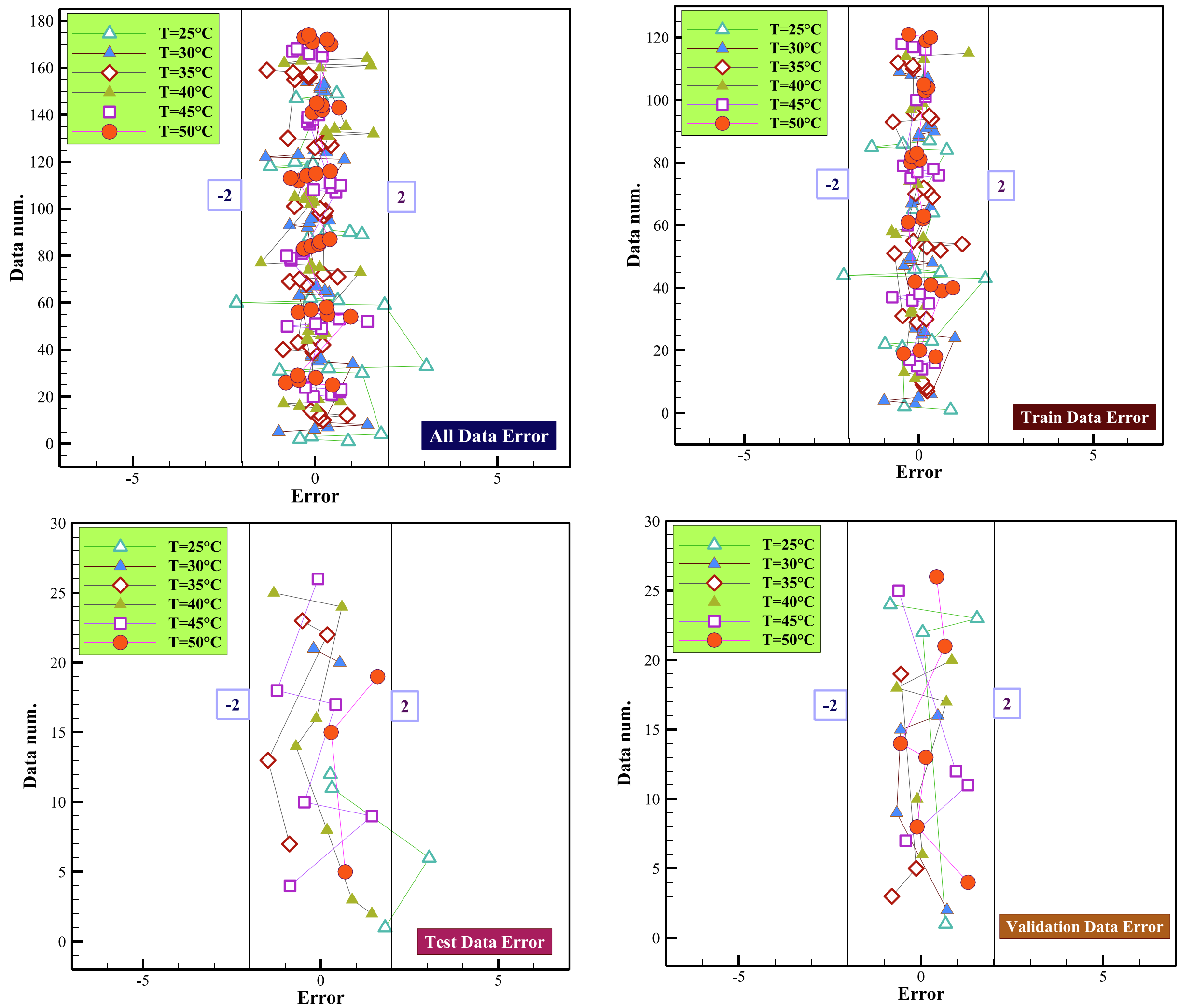

Fig. 10 Calculated error values.

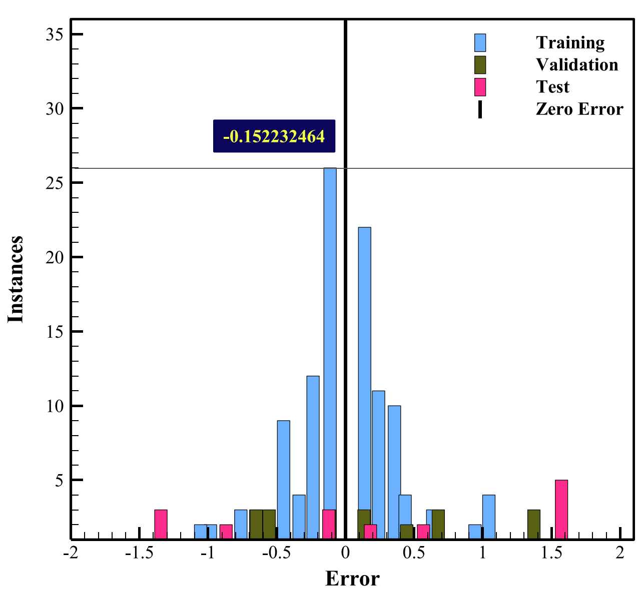

Fig. 11 Histogram plot.

The margin of deviation (MOD) for the experimental information is reported with the predicted data for the different phases in Eq. (2).

$$MOD(\%) = \frac{\mu_{pre-}\mu_{exp}}{\mu_{exp}} \times 100 \tag{2}$$

Fig. 11 displays the MOD of this information at various φ. According to Fig. 11, the MOD does not surpass 1 % ±, which shows a satisfactory precision of the association accuracy of the proposed data for forecasting the μ_{nf} of MWCNT-MgO (25:75) / SAE40 NL. The highest MOD in all information phase at T = 40 ^{0}C was observed in the range of less than −2%. In other phases, it has the lowest MOD.

To predict the μ_{nf} of MWCNT-MgO (25:75)/SAE40 NL, the Batchelor relation (Eq. (3) was offered, which is according to the φ and the base fluid viscosity and estimates the μ_{nf}. This relationship is defined as follows Batchelor (1977):

$$\mu_{nf} = (1 + 2.5\varphi + 6.5\varphi^2)\mu_f \tag{3}$$

Fig. 13 displays the ultimate comparison of the study, which is very significant. In this sector, the outputs of the reported relationship, the ANN prediction data and the μ_{nf}

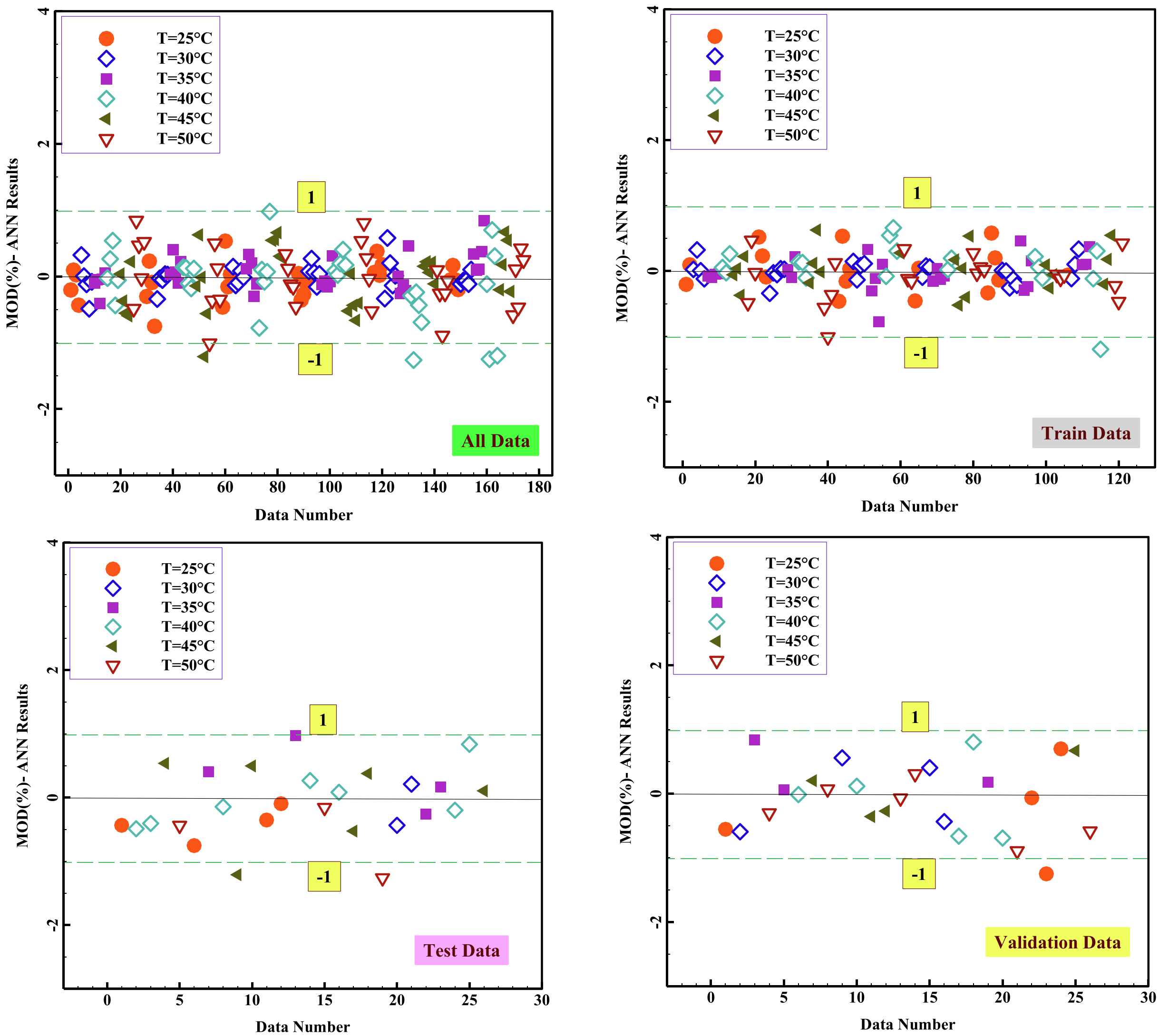

Fig. 12 MOD charts.

of the experimental data at different φ and T = 25, 30, 40 and 50 °C and$\dot{\gamma}$ = 3999 s^{-1} are compared. Comparisons show that there is satisfactory compatibility between the considered ANN outputs and the experimental results. ANN accuracy proves the consistency of the μ_{nf} of ANN data and experimental data. In addition, the obtained values from the presented relationship to predict the μ_{nf} at high φ are close to the outcomes of laboratory data, but their precision is less than the ANN.

4. Conclusion

Examining laboratory data for μ_{nf} takes a lot of time and money. As a result, several techniques were proposed to predict the μ_{nf}. One of the best methods is data modeling by ANN. In this work, μ_{nf} of MWCNT-MgO/SAE40 NL was evaluated using ANN. Also, 174 laboratory data in terms of temperature, $\dot{\gamma}$ and φ were used for ANN modeling. Temperature, $\dot{\gamma}$ and φ were considered as input variables and predicted μ_{nf} as output variables in ANN. In this research, the MLP model with an LM algorithm with two transfer functions was used to design ANN. The RC and MSE for the ANN operating system were 0.9999882 and 0.001453292, respectively. The operating system is selected from among 400 ANN samples that have two HLs and 8 and 5 neurons in the first and second HLs. The highest frequency of MOD Amounts was in the range of $-1 < \text{MOD} > +1$, indicating a very low error of ANN data for μ_{nf}. In the final part, the comparison of three groups of data, i.e., Experimental data, correlation output and ANN predicted data show that ANN performed better in predicting μ_{nf} than the presented relationship. Therefore, the predicted data are more accurate than the calculated data. The main goal of the present work is to design, model, and estimate the viscosity of MWCNT-MgO/SAE40 NL through ANN artificial neural network and Choosing the best and most suitable optimal structure from the set of ANN predicted structures is financially and laboratory work time wise.

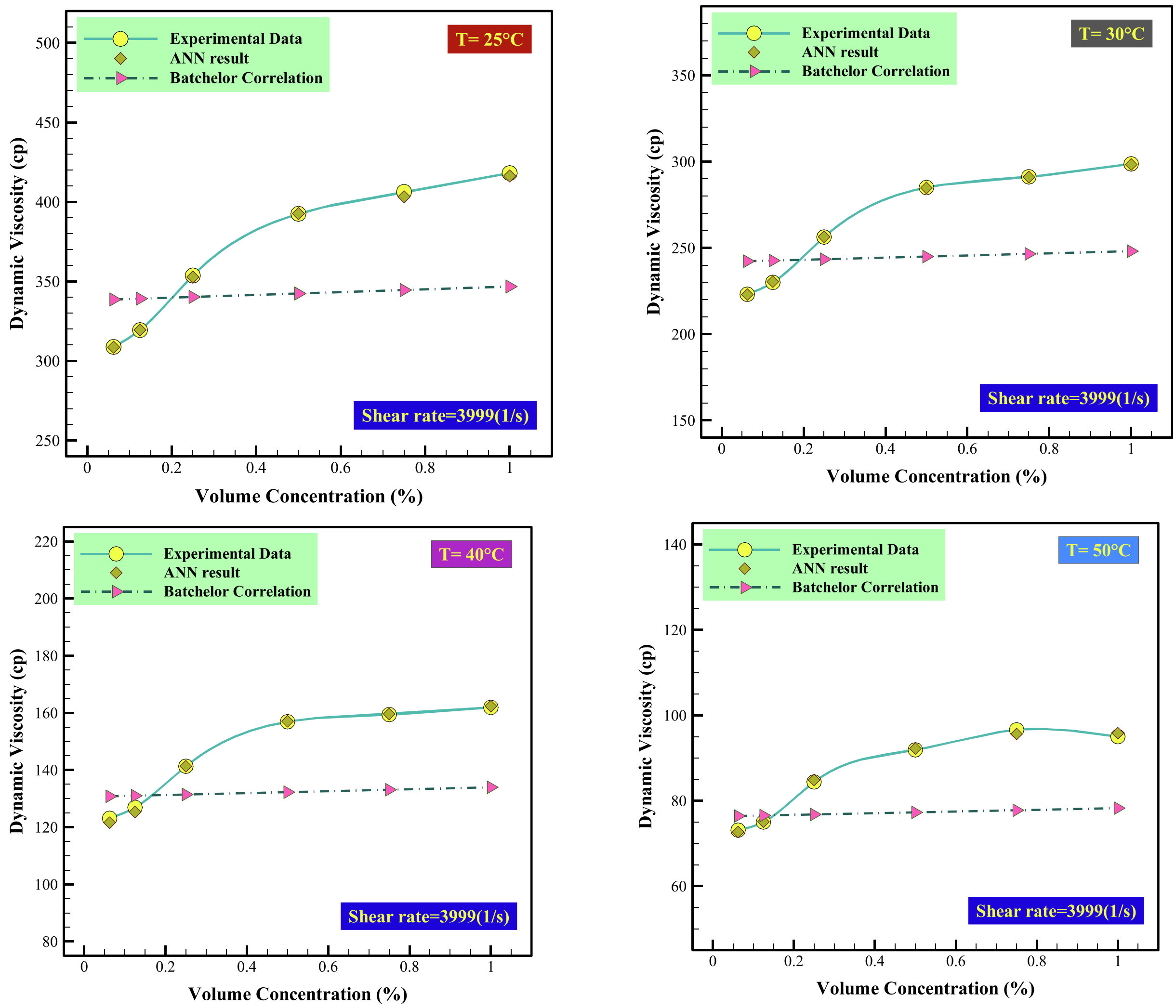

Fig. 13 Comparison among empirical information (Zhang et al., 2022b) and modeling outputs of ANN and association.

Declaration of Competing Interest

The authors declare that they have no known competing financial interests or personal relationships that could have appeared to influence the work reported in this paper.

References

Aberoumand, S., Jafarimoghaddam, A., Moravej, M., Aberoumand, H., Javaherdeh, K., 2016. Experimental study on the rheological behavior of silver-heat transfer oil nanofluid and suggesting two empirical based correlations for thermal conductivity and viscosity of oil based nanofluids. Appl. Therm. Eng. 101, 362–372.

Afrand, M., Nadooshan, A.A., Hassani, M., Yarmand, H., Dahari, M., 2016. Predicting the viscosity of multi-walled carbon nanotubes/water nanofluid by developing an optimal artificial neural network based on experimental data. Int. Commun. Heat Mass Transfer 77, 49–53.

Aghaei, A., Khorasanizadeh, H., Sheikhzadeh, G.A., 2018. Measurement of the dynamic viscosity of hybrid engine oil-Cuo-MWCNT nanofluid, development of a practical viscosity correlation and utilizing the artificial neural network. Heat Mass Transf. 54 (1), 151–161.

Akhavan-Behabadi, M.A., Hekmatipour, F., Sajadi, B., 2016. An empirical study on the mixed convection transfer and pressure drop of HTO/CuO nanofluid in inclined tubes. Exp. Therm Fluid Sci. 78, 10–17.

Alidoust, S., AmoozadKhalili, F., Hamedi, S., 2022. Investigation of effective parameters on relative thermal conductivity of SWCNT (15%)-Fe_3O_4 (85%)/water hybrid ferro-nanofluid and presenting a new correlation with response surface methodology. Colloids Surf., A: Physicochem. Eng. Aspects 645, 128625.

Anqi, A.E., Li, C., Dhahad, H.A., Sharma, K., Attia, E.A., Abdelrahman, A., Rajhi, A.A., 2022. Effect of combined air cooling and nano enhanced phase change materials on thermal management of lithium-ion batteries. J. Storage Mater. 52, 104906.

Ashrafi, M., Bagherian, G., Chamjangali, M.A., Goudarzi, N., 2018. Application of artificial neural network and random forest methods for modeling simultaneous adsorption of safranin-O and methyl violet dyes onto modified pine cone powder. Desalin. Water Treat. 109, 90–103.

Azin, Z., Pourghobadi, Z., 2021. Electrochemical sensor based on nanocomposite of multi-walled carbon nano-tubes (MWCNTs)/TiO_2/Carbon ionic liquid electrode analysis of acetaminophen in pharmaceutical formulations. Iran. J. Chem. Chem. Eng. Research Article 40 (4).

Azman, A., Yusoff, M.Z., Mukhtar, A., Gunnasegaran, P., Hamid, N. A., Ching, N.K., 2021. Numerical study of heat transfer enhancement for mono and hybrid nanofluids flow in a straight pipe. CFD Lett. 13 (2), 49–61.

Bagheri, M., Lesiuk, G., de Oliveira Correia, J.A.F., 2020. Seismic hydro-dynamic analysis of pipes with internal and external fluid under nanoparticles as reinforcement phase. Int. J. Hydromechatronics 3 (3), 252–267.

Banisharif, A., Estellé, P., Rashidi, A., Van Vaerenbergh, S., Aghajani, M., 2021. Heat transfer properties of metal, metal oxides, and carbon water-based nanofluids in the ethanol condensation process. Colloids Surf., A: Physicochem. Eng. Aspects 622, 126720.

Barati-Harooni, A., Najafi-Marghmaleki, A., 2016. An accurate RBF-NN model for estimation of viscosity of nanofluids. J. Mol. Liq. 224, 580–588.

Batchelor, G.K., 1977. The effect of Brownian motion on the bulk stress in a suspension of spherical particles. J. Fluid Mech. 83 (1), 97–117.

Binu, K.G., Spoorthi, M., Prajwal, K., Vaz, N., D'Silva, R., Pai, R., 2015. Formulation and viscosity analysis of TiO_2 nanoparticle dispersions in engine oil. Am J Mater Sci 5 (3C), 198–202.

Çolak, A.B., 2021. A novel comparative analysis between the experimental and numeric methods on viscosity of zirconium oxide nanofluid: Developing optimal artificial neural network and new mathematical model. Powder Technol. 381, 338–351.

Dezfulizadeh, A., Aghaei, A., Joshaghani, A.H., Najafizadeh, M.M., 2021. An experimental study on dynamic viscosity and thermal conductivity of water-Cu-SiO_2-MWCNT ternary hybrid nanofluid and the development of practical correlations. Powder Technol. 389, 215–234.

Dianati Tilaki, G.A., Ahmadi Jolandan, M., Gholami, V., 2020. Rangelands production modeling using an artificial neural network (ANN) and geographic information system (GIS) in Baladeh rangelands, North Iran. Caspian J. Environ. Sci. 18 (3), 277–290.

Domyati, D., 2022. Characterization of biofabrication copper (ii) oxide nanoparticles and investigate the photocatalytic efficiency. Eur. Chem. Bull. 11 (2), 1–6.

Dongale, T.D., Jadhav, P.R., Navathe, G.J., Kim, J.H., Karanjkar, M. M., Patil, P.S., 2015. Development of nano fiber MnO_2 thin film electrode and cyclic voltammetry behavior modeling using artificial neural network for supercapacitor application. Mater. Sci. Semicond. Process. 36, 43–48.

Einstein, A., 1905. Eine neue bestimmung der moleküldimensionen, Doctoral dissertation, ETH Zurich.

Esfe, M.H., 2017. Designing an artificial neural network using radial basis function (RBF-ANN) to model thermal conductivity of ethylene glycol–water-based TiO2 nanofluids. Journal of Thermal Analysis and Calorimetry 127, 2125–2131.

Esfe, M.H., Arani, A.A.A, 2018. An experimental determination and accurate prediction of dynamic viscosity of MWCNT (% 40)-SiO2 (% 60)/5W50 nano-lubricant. Journal of Molecular Liquids 259, 227–237.

Esfe, M.H., Saedodin, S., 2014. An experimental investigation and new correlation of viscosity of ZnO–EG nanofluid at various temperatures and different solid volume fractions. Experimental thermal and fluid science 55, 1–5.

Esfe, M.H., Rostamian, H., Sarlak, M.R., 2018. A novel study on rheological behavior of ZnO-MWCNT/10w40 nanofluid for automotive engines. Journal of Molecular Liquids 254, 406–413.

Esfe, M.H., Saedodin, S., Asadi, A., 2014. An empirical investigation on the dynamic viscosity of Mg (OH) 2-ethylene glycol in different solid concentrations and proposing new correlation based on experimental data. Int. J. Nat. Eng. Sci. 8 (3), 29–34.

Esfe, M.H., Sarlak, M.R., 2017. Experimental investigation of switchable behavior of CuO-MWCNT (85%–15%)/10W-40 hybrid nano-lubricants for applications in internal combustion engines. Journal of Molecular Liquids 242 (2), 326–335.

Fontes, D.H., Ribatski, G., Bandarra Filho, E.P., 2015. Experimental evaluation of thermal conductivity, viscosity and breakdown voltage AC of nanofluids of carbon nanotubes and diamond in transformer oil. Diam. Relat. Mater. 58, 115–121.

Ghazvini, M., Maddah, H., Peymanfar, R., Ahmadi, M.H., Kumar, R., 2020. Experimental evaluation and artificial neural network modeling of thermal conductivity of water based nanofluid containing magnetic copper nanoparticles. Physica A 551, 124127.

Goudarzi, N., Goodarzi, M., 2008. Prediction of the logarithmic of partition coefficients (log P) of some organic compounds by least square-support vector machine (LS-SVM). Mol. Phys. 106 (21–23), 2525–2535.

Goudarzi, N., Goodarzi, M., 2009. Prediction of the vapor pressure of some halogenated methyl-phenyl ether (anisole) compounds using linear and nonlinear QSPR methods. Mol. Phys. 107 (15), 1615–1620.

Haddad, Z., Hakan, F., Oztop, A.-N., Mataoui, A., 2012. A review on natural convective heat transfer of nanofluids. Renew. Sustain. Energy Rev. 12 (7), 5363–5378.

He, W. et al, 2020. Using of artificial neural networks (ANNs) to predict the thermal conductivity of zinc oxide–silver (50%–50%)/ water hybrid Newtonian nanofluid. Int. Commun. Heat Mass Tran. 116.

Hemmat Esfe, M., Toghraie, D., Alidoust, S., Amoozad, F., ardeshiri, E.M, 2022. Investigating the rheological behavior of a hybrid nanofluid (HNF) to present to the industry. Heliyon.

Hosseini, S.M.S., Dehaj, M.S., 2021a. An experimental study on energetic performance evaluation of a parabolic trough solar collector operating with Al_2O_3/water and GO/water nanofluids. Energy 234, 121317.

Hosseini, S.M.S., Dehaj, M.S., 2021b. Assessment of TiO2 water-based nanofluids with two distinct morphologies in a U type evacuated tube solar collector. Appl. Therm. Eng. 182, 116086.

Jamei, M., Olumegbon, I.A., Karbasi, M., Ahmadianfar, I., Asadi, A., Mosharaf-Dehkordi, M., 2021. On the Thermal Conductivity Assessment of Oil-Based Hybrid Nanofluids using Extended Kalman Filter integrated with feed-forward neural network. Int. J. Heat Mass Transf. 172, 121159.

Jamil, F., Muhammad, H., 2020. Applications of hybrid nanofluids in different fields. Elsevier Inc..

Keshtegar, B., Correia, J.A.F.O., Trung, N.-T., 2020. Optimisation of nanocomposite pipes under internal fluid reinforced by FRP and CNTs under seismic load. Int. J. Hydromechatronics 3 (3), 213–227.

Khanafer, K., Vafai, K., 2012. A critical synthesis of thermophysical characteristics of nanofluids. Int. J. Heat Mass Transf. Volume 54, Issue 19–20, 4410–4428.

Kotia, A., Ghosh, S.K., 2015. Experimental analysis for rheological properties of aluminium oxide (Al_2O_3)/gear oil (SAE EP-90) nanolubricant used in HEMM. Ind. Lubrication Tribol.

Krieger, I.M., Dougherty, T.J., 1959. A mechanism for non-Newtonian flow in suspensions of rigid spheres. Trans. Soc. Rheol. 3 (1), 137–152.

Li, H., Zhang, Y., Li, C., Zhou, Z., Nie, X., Chen, Y., Sharma, S., 2022. Extreme pressure and antiwear additives for lubricant: academic insights and perspectives. Int. J. Adv. Manuf. Technol., 1–27

Lundgren, T.S., 1972. Slow flow through stationary random beds and suspensions of spheres. J. Fluid Mech. 51 (2), 273–299.

Meybodi, M.K., Daryasafar, A., Koochi, M.M., Moghadasi, J., Meybodi, R.B., Ghahfarokhi, A.K., 2016. A novel correlation approach for viscosity prediction of water based nanofluids of Al_2O_3, TiO_2, SiO_2 and CuO. J. Taiwan Inst. Chem. Eng. 58, 19–27.

Mousavi, S.M., Ehteshami, B., Darzi, A.A.R., 2021. Two-and-three-dimensional analysis of Joule and viscous heating effects on MHD nanofluid forced convection in microchannels. Thermal Science and Engineering Progress 25, 100983.

Nfawa, S.R., Basri, A.A., Masuri, S.U., 2021. Novel use of MgO nanoparticle additive for enhancing the thermal conductivity of CuO/water nanofluid. Case Stud. Therm. Eng. 101279.

Nielsen, L.E., 1970. Generalized equation for the elastic moduli of composite materials. J. Appl. Phys. 41 (11), 4626–4627.
Öğüt, E.B., Kahveci, K., 2016. Mixed convection heat transfer of ethylene glycol and water mixture based Al2O3 nanofluids: effect of thermal conductivity models. J. Mol. Liq. 224, 338–345.
Putra, A.B.W., 2020. Computer technology simulation towards power generation potential from coproduced fluids in South Lokichar oil fields. Int. J. Commun. Computer Technologies 8 (2), 9.
Rezaee, M.J., Jozmaleki, M., Valipour, M., 2018. Integrating dynamic fuzzy C-means, data envelopment analysis and artificial neural network to online prediction performance of companies in stock exchange. Physica A: Statistical Mech. its Applications 489, 78–93.
Rikani, A.S., 2021. Investigation of turbulent fluid flow in the presence of a magnetic field induced dynamic motion of the vessel. J. Res. Sci. Eng. Technol. 9 (01), 74–94.
Ruhani, B., Toghraie, D., Hekmatifar, M., Hadian, M., 2019a. Statistical investigation for developing a new model for rheological behavior of ZnO–Ag (50%–50%)/Water hybrid Newtonian nanofluid using experimental data. Physica A: Statistical Mech. its Applications 525, 741–751.
Ruhani, B. et al, 2022. Statistical modeling and investigation of thermal characteristics of a new nanofluid containing cerium oxide powder. Heliyon e11373.
Ruhani, B., Barnoon, P., Toghraie, D., 2019b. Statistical investigation for developing a new model for rheological behavior of Silica–ethylene glycol/Water hybrid Newtonian nanofluid using experimental data. Physica A: Statistical Mech. its Applications 525, 616–627.
Rustamovich Sultanbekov, I., Yurievna Myshkina, I., Yurievna Gruditsyna, L., 2020. Development of an application for creation and learning of neural networks to utilize in environmental sciences. Caspian J. Environ. Sci. 18 (5), 595–601.
Safa, M., Ahmadi, M., Mehrmashadi, J., Petkovic, D., Mohammadhassani, M., Zandi, Y., Sedghi, Y., 2020. Selection of the most influential parameters on vectorial crystal growth of highly oriented vertically aligned carbon nanotubes by adaptive neuro-fuzzy technique. Int. J. Hydromechatronics 3 (3), 238–251.
Saidur, R., Leong, K.Y., Mohammad, 2011. A review on applications and challenges of nanofluids. Renew. Sustain. Energy Rev. 15, 1646–1668.
Shaddel, M., Javan, D.S., Baghernia, P., 2016. Estimation of hourly global solar irradiation on tilted absorbers from horizontal one using Artificial Neural Network for case study of Mashhad. Renew. Sustain. Energy Rev. 53, 59–67.
Shahsavar, A., Jamei, M., Karbasi, M., 2021. Experimental evaluation and development of predictive models for rheological behavior of aqueous Fe3O4 ferrofluid in the presence of an external magnetic field by introducing a novel grid optimization based-Kernel ridge regression supported by sensitivity analysis. Powder Technol.
Shakeri, S., Ghassemi, A., Hassani, M., Hajian, A., 2016. Investigation of material removal rate and surface roughness in wire electrical discharge machining process for cementation alloy steel using artificial neural network. Int. J. Adv. Manuf. Technol. 82 (1–4), 549–557.
Sheikholeslami, M., 2017. Influence of Lorentz forces on nanofluid flow in a porous cylinder considering Darcy model. J. Mol. Liq. 225, 903–912.
Shirani, M., Akbari, A., Hassani, M., 2015. Adsorption of cadmium (ii) and copper (ii) from soil and water samples onto a magnetic organozeolite modified with 2-(3, 4-dihydroxyphenyl)-1, 3-dithiane using an artificial neural network and analysed by flame atomic absorption spectrometry. Anal. Methods 7 (14), 6012–6020.
Sutar, S.S., Patil, S.M., Kadam, S.J., Kamat, R.K., Kim, D.K., Dongale, T.D., 2021. Analysis and prediction of hydrothermally synthesized ZnO-Based dye-sensitized solar cell properties using statistical and machine-learning techniques. ACS Omega 6 (44), 29982–29992.
Tan, X., Obaid, R.F., Smaisim, G.F., Esfahani, M.M., Alsaikhan, F., Baghaei, S., Yadav, A., 2022. Investigation of addition of calcium phosphate ceramic to multilayer scaffold for bone applications with improved mechanical properties: fuzzy logic analysis. Ceramics International.
Tang, L., Zhang, Y., Li, C., Zhou, Z., Nie, X., Chen, Y., Sharma, S., 2022. Biological stability of water-based cutting fluids: progress and application. Chinese J. Mech. Eng. 35 (1), 1–24.
Tseng, W.J., Chen, C.N., 2003. Effect of polymeric dispersant on rheological behavior of nickel–terpineol suspensions. Mater. Sci. Eng., A 347 (1–2), 145–153.
Valipour, P., Aski, F.S., Mirparizi, M., 2017. Influence of magnetic field on CNT-Polyethylene nanofluid flow over a permeable cylinder. J. Mol. Liq. 225, 592–597.
Wang, X., Xu, X., Choi, S.U., 1999. Thermal conductivity of nanoparticle-fluid mixture. J. Thermophys Heat Transfer 13 (4), 474–480.
Wang, X., Li, C., Zhang, Y., Said, Z., Debnath, S., Sharma, S., Gao, T., 2022. Influence of texture shape and arrangement on nanofluid minimum quantity lubrication turning. Int. J. Adv. Manuf. Technol. 119 (1), 631–646.
Yan, Q., Wang, B., Gong, D., Luo, C., Zhao, W., Shen, J., You, Z., 2020. COVID-19 chest CT image segmentation–a deep convolutional neural network solution. arXiv preprint arXiv:2004.10987.
Yang, X., Boroomandpour, A., Wen, S., Toghraie, D., Soltani, F., 2021. Applying Artificial Neural Networks (ANNs) for prediction of the thermal characteristics of water/ethylene glycol-based mono, binary and ternary nanofluids containing MWCNTs, titania, and zinc oxide. Powder Technol. 388, 418–424.
Yang, M., Li, C., Zhang, Y., Jia, D., Zhang, X., Hou, Y., Wang, J., 2017. Maximum undeformed equivalent chip thickness for ductile-brittle transition of zirconia ceramics under different lubrication conditions. Int. J. Mach. Tools Manuf 122, 55–65.
Zhang, G., Chen, J., Zhang, Z., Sun, M., Yu, Y., Wang, J., Cai, S., 2022a. Analysis of magnetorheological clutch with double cup-shaped gap excited by Halbach array based on finite element method and experiment. Smart Mater. Struct.
Zhang, Y., Li, C., Jia, D., Zhang, D., Zhang, X., 2015. Experimental evaluation of the lubrication performance of MoS2/CNT nanofluid for minimal quantity lubrication in Ni-based alloy grinding. Int. J. Mach. Tools Manuf 99, 19–33.
Zhang, Y., Junwen, X., Pengfei, F., et al, 2021. Optimization design of radiator for armored vehicle based on RBF neural network. J. Ordnance Equipment Eng. 42 (02), 68–75.
Zhang, G., Zhang, Z., Sun, M., Yu, Y., Wang, J., Cai, S., 2022b. The influence of the temperature on the dynamic behaviors of magnetorheological gel. Adv. Eng. Mater. 2101680.